Mon. Not. R. Astron. Soc. **381,** 125–135 (2007) doi:10.1111/j.1365-2966.2007.12213.x

Neon and argon optical emission lines in ionized gaseous nebulae: implications and applications

Enrique Pérez-Montero,[1,2]★† Guillermo F. Hägele,[2]‡ Thierry Contini[1] and Ángeles I. Díaz[2]§

[1]*Laboratoire d'Astrophysique de Toulouse et Tarbes (UMR 5572), Observatoire Midi-Pyrénées 14, avenue Edouard Belin, F-31400 Toulouse, France*
[2]*Departamento de Física Teórica, C-XI, Universidad Autónoma de Madrid, 28049 Madrid, Spain*

Accepted 2007 July 5. Received 2007 July 5; in original form 2007 May 25

ABSTRACT

In this work, we present a study of the strong optical collisional emission lines of Ne and Ar in an heterogeneous sample of ionized gaseous nebulae for which it is possible to derive directly the electron temperature and hence the chemical abundances of Ne and Ar. We calculate using a grid of photoionization models new ionization correction factors for these two elements and we study the behaviour of Ne/O and Ar/O abundance ratios with metallicity. We find a constant value for Ne/O, while there seems to be some evidence for the existence of negative radial gradients of Ar/O over the discs of some nearby spirals. We study the relation between the intensities of the emission lines of [Ne III] at 3869 Å and [O III] at 4959 and 5007 Å. This relation can be used in empirical calibrations and diagnostic ratios extending their applicability to bluer wavelengths and therefore to samples of objects at higher redshifts. Finally, we propose a new diagnostic using [O II], [Ne III] and Hδ emission lines to derive metallicities for galaxies at high z.

Key words: ISM: abundances – H II regions.

1 INTRODUCTION

The chemical history of the Universe can be investigated by studying the behaviour of abundance ratios of different chemical species as a function of metallicity, which is the main indicator of the chemical evolution of a galaxy. If two elements are produced by stars of the same mass range, they will appear simultaneously in the interstellar medium (ISM) and hence their relative abundance will be constant. However, if they are produced by stars of different mass ranges, they will be ejected into the ISM in different time-scales. The chemical abundances of the elements heavier than hydrogen can be studied by measuring the fluxes of the absorption and emission lines in the spectra of stars and galaxies. Unluckily, only the collisional emission lines emitted by the ionized gas surrounding massive star clusters are detectable in most of galaxies. Since the brightest emission lines in the optical part of the spectrum are emitted by oxygen, this element has been taken as the main tracer of metallicity for these objects. Nevertheless, the depletion of some of the most important elements, including oxygen, on to dust grains, whose composition is difficult to ascertain, makes the determination of these abundances more uncertain. This is not the case for the elements that occupy the last group in the periodic table, that have an electronic configuration with the outer shell completely filled and they seldom associate to other elements and do not constitute part of the dust grains in the ISM. Therefore, although the presence of these grains can affect the determination of metallicity in other ways, affecting the photoionization equilibrium of the gas, the uncertainty due to depletion factors has not to be considered in the determination of the chemical abundances of the noble gases.

Ne and Ar are products of the late stages in the evolution of massive stars. Ne is produced by carbon burning and is expected to track oxygen abundances very closely. The measurement of Ne abundances in extragalactic H II regions (Garnett 2002) and planetary nebulae (Henry 1989) confirms this trend, despite the uncertainties in the derivation of the ionization correction factor (ICF) of Ne. On the other hand, Ar, like sulphur, is produced by oxygen burning and, again, it is expected to track O abundances. Nevertheless, as it is also the case for sulphur, there is some evidence of decreasing values of Ar/O for higher metallicities (Garnett 2002). The same trend has been observed for sulphur in halo metal-poor stars (Israelian & Rebolo 2001) and extragalactic H II regions (Díaz et al. 1991; Garnett 2002; Pérez-Montero et al. 2006). This problem, perhaps, is related to the proximity of the production site of these elements to the stellar core and the yields would be sensitive to the conditions during the supernova explosion (Weaver & Woosley 1993).

The emission lines of Ne and Ar are not as intense as some of the other strong lines in the optical spectrum but there is a growing

★Postdoctorate Fellow of the Ministerio de Educación y Ciencia, Spain.
†E-mail: enrique.perez@ast.obs-mip.fr
‡PhD Fellow of the Ministerio de Educación y Ciencia, Spain.
§On sabbatical leave at the Institute of Astronomy, Cambridge.

number of H II regions for which there are measurements with good signal-to-noise ratio (S/N). This is the case of [Ne III] at 3869 Å, whose blue wavelength makes it observable in the optical spectrum of bright objects, even at high redshifts, and the emission line of [Ar III] at 7136 Å. The emission lines of these elements in the infrared (IR) will supply a great deal of worthy additional information but, at this moment, the objects with observations of the fine-structure lines of [Ne II], [Ne III], [Ar II] and [Ar III] are still very scarce. The derivation of the chemical abundances of these elements in H II regions can be calculated by means of the previous determination of some electron collisional temperature and the previous knowledge of the ionization structure of the element whose abundance is required. The results of photoionization models point to a similar ionization structure of Ne and O, on the one hand, and S and Ar, on the other (e.g. Pérez-Montero & Díaz 2007). These facts make these lines suitable to be used as substitutes of the bright emission lines of oxygen and sulphur in empirical indicators of metallicity (e.g. Nagao, Maiolino & Marconi 2006) or diagnostic ratios to distinguish starburst galaxies from active galactic nuclei (AGN) (e.g. Rola, Terlevich & Terlevich 1997).

In this paper, we investigate the element abundances of Ne, Ar and oxygen for a sample of objects that is described in Section 2. In Section 3, we derive the physical conditions of these objects, including the calculation of the electron temperatures involved in the derivation of Ne and Ar abundances. In Section 4, we describe the grid of photoionization models that we have used to derive a new set of ICFs for these two elements. These new ICFs are described in the next section, along with the discussion of the behaviour of Ne/O and Ar/O ratios and the use of the brightest emission lines of these two elements as empirical calibrators of metallicity and diagnostic ratios. Finally, we summarize our results and we present our conclusions.

2 DESCRIPTION OF THE SAMPLE

The sample includes emission-line objects observed in the optical part of the spectrum with the detection of, at least, one auroral line with high S/N in order to derive electron temperatures directly and, hence, ionic chemical abundances with less uncertainty. We have compiled for this sample the strong lines of [O II] at 3727 Å and [O III] at 4959 and 5007 Å in order to derive oxygen abundances. We have compiled as well the [Ne III] emission line at 3869 Å, the [Ar III] emission line at 7136 Å and the [Ar IV] emission line at 4740 Å to measure the respective ionic abundances of Ne and Ar. The compilation includes the objects used in Pérez-Montero & Díaz (2005), including H II regions in our Galaxy and the Magellanic Clouds, giant extragalactic H II regions (GEHRs) and H II galaxies, with the addition of new objects which are listed in Table 1.

This list includes 12 H II galaxies from the Sloan Digital Sky Survey (SDSS[1]) with very low metallicities identified by Kniazev et al. (2003) and whose spectra have been re-analysed to obtain the required line emission data. Among these galaxies, 11 do not have observations of the [O II] emission line at 3727 Å, which is the case as well for 183 SDSS galaxies of the sample compiled by Izotov et al. (2006). The compilation has therefore 633 H II galaxies, 176 GEHRs and 44 H II regions of the Galaxy and the Magellanic Clouds with a good determination of oxygen, Ne and Ar ionic abundances for those ions that have been observed.

[1] The SDSS site is at www.sdss.org.

Table 1. Bibliographic references for the emission-line fluxes of the compiled sample.

Reference	Object type[a]	Objects
Bresolin et al. (2004)	M51 GEHRs	10
Bresolin et al. (2005)	GEHRs	32
Bresolin (2007)	M101 GEHRs	3
Crockett, Garnett & Jacoby (2006)	M33 GEHRs	6
Garnett et al. (2004)	M51 GEHRs	2
Guseva et al. (2003a)	SBS 1129+576	2
Guseva et al. (2003b)	HS 1442+650	2
Guseva et al. (2003c)	SBS 1415+437	2
Hägele et al. (2006)	HIIG	3
Hägele et al. (2007)	HIIG	7
Izotov et al. (1997)	IZw18	2
Izotov & Thuan (1998)	SBS 0335−018	1
Izotov et al. (1999)	H IIG	3
Izotov, Chaffee & Green (2001)	H IIG	2
Izotov et al. (2004a)	H IIG	3
Izotov & Thuan (2004)	H IIG	33
Izotov et al.	SDSS galaxies	309
Kniazev et al.	SDSS galaxies	11
Lee, Salzer & Melbourne (2004)	KISS galaxies	13
Melbourne et al. (2004)	KISS galaxies	12
Pérez-Montero & Díaz (2005)	All	361
van Zee (2000)	UGCA92	2
Vermeij et al. (2002)	DHR	5

[a]GEHRs denote giant extragalactic H II regions, H IIGs denote H II galaxies and DHR denotes diffuse H II regions.

The emission-line intensities have been taken directly from the literature once reddening corrected. The aperture effects of all the compiled observations are negligible due to the compact nature of the observed objects and the high-excitation state of the more important involved emission lines.

3 PHYSICAL CONDITIONS

3.1 Electron density and temperatures

In order to derive oxygen, Ne and Ar abundances for the ions presenting the corresponding strong emission line, we have selected objects allowing a direct determination of the electron temperature. All physical conditions have been derived from the appropriate ratios of emission lines and using fittings to the values obtained with the task TEMDEN, in the case of electron densities and temperatures, and IONIC, in the case of ionic abundances of the software package IMAGE REDUCTION AND ANALYSIS FACILITY (IRAF)[2] and which are based on the five-level statistical equilibrium model (De Robertis, Dufour & Hunt 1987; Shaw & Dufour 1995). The references for the collision strengths of the ions involved in our calculations are listed in Table 2.

Next, following the same procedure described in Pérez-Montero & Díaz (2003), we have used for the calculation of the chemical abundance the electron temperature associated with the zone where each ionic species stays. To do this we have applied different expressions for the relations between the electron temperatures of each zone.

Electron densities have been calculated for a subsample of 361 objects from the ratio of [S II] emission lines $I(6717\ \text{Å})/I(6731\ \text{Å})$. It

[2] IRAF (Image Reduction and Analysis Facility) is distributed by the National Optical Astronomical Observatory.

Table 2. Bibliographic references for the collision strengths of the forbidden lines for each ion.

Ion	Reference
O II	Pradhan (1976)
O III	Lennon & Burke (1994)
Ne III	Butler & Zeippen (1994)
S II	Ramsbottom, Bell & Stafford (1996)
S III	Tayal & Gupta (1999)
Ar III	Galavis, Mendoza & Zeippen (1995)
Ar IV	Zeippen, Le Bourlot & Butler (1987)

is representative of the low-excitation zone of the ionized gas, and it is therefore used for the calculation of electron temperatures in this zone which depend on density. For the remaining the objects, for which no data about [S II] lines exist or for which they give non-valid values, we have considered a mean density of 50 particles per cm^3, according to the low-density values found in the rest of H II regions.

The electron temperature of O^{2+}, representative of the high-excitation zone of the ionized gas, has been derived from the ratio of [O III] emission lines (I(4959 Å)+I(5007))/I(4363 Å) for a subsample of 771 objects, while for the rest we have used the relation with other measured electron temperatures in an inverse way as described below: 33 from t([S III]), 20 from t([O II]) and finally four from t([N II]). In the latter case, the objects are M51 GEHRs of high metallicity from Bresolin, Garnett & Kennicutt (2004). We have assumed as well t([O III]) to be equal to t([Ne III]) and t([Ar IV]) in order to calculate Ne^{2+} and Ar^{3+} abundances, respectively.

The electron temperature of O^+, representative of the low-excitation zone of the ionized gas, has been derived from the ratio of the [O II] emission lines [I(3727 Å)/I(7319 Å)+I(7330 Å)] for a subsample of 311 objects. The auroral lines of [O II] present higher uncertainties because of their lower S/N and a higher dependence on reddening correction, due to their larger wavelength distance to the closest hydrogen recombination emission line. Besides, they present a small contribution due to recombination, although in quantities not larger than the usual reported errors. Additionally, this ratio has a strong dependence on electron density, which makes the determination of this temperature and, hence, the determination of O^+ abundances very uncertain. This can increase the uncertainty of total oxygen abundances, mostly in high-metallicity, low-excitation H II regions (Pérez-Montero & Díaz 2005). For the rest of the objects, we have used the grid of relations between t([O II]) and t([O III]) presented in Pérez-Montero & Díaz (2003), which takes into account the dependence of t([O II]) on density and its corresponding uncertainty. For the same four objects of M51 for which neither t([O III]) nor t([S III])] have been measured, we have taken t([N II]) as a representative of the electron temperature of the low-excitation zone using the ratio of [N II] emission lines [I(6548 Å)+I(6584 Å)]/I(5755 Å).

In the case of the electron temperature of Ar^{2+}, we have assumed that the ionization structure of this ion is rather similar to that of S^{2+}, whose electron temperature has intermediate values between the high- and low-excitation zones (Garnett 1992). We have calculated directly the temperature of S^{2+} from the ratio of [S III] emission lines [I(9069 Å)+I(9532 Å)]/I(6312 Å) for a subsample of 299 objects. For the rest of the objects, we have taken relations of this temperature with t([O III]). In the case of low-excitation objects ($T_e < 10\,000$ K), based on photoionization models (Pérez-Montero & Díaz 2005):

$$t([\mathrm{S\,III}]) = 1.05t([\mathrm{O\,III}]) - 0.08 \quad (1)$$

while for the high-excitation objects we have taken the empirical relation found by Hägele et al. (2006) that accounts better for the high dispersion found in this relation for H II galaxies:

$$t([\mathrm{S\,III}]) = (1.19 \pm 0.08)t([\mathrm{O\,III}]) - (0.32 \pm 0.10). \quad (2)$$

3.2 Ionic abundances

Each ionic abundance has been calculated using the most prominent emission lines for each ion and the appropriate electron temperature. In the case of O^+, we have used the following expression using the intensity of the [O II] line at 3727 Å, the electron temperature t([O II]), or any other value associated to the low-excitation zone and the electron density, n:

$$12 + \log\left(\frac{\mathrm{O^+}}{\mathrm{H^+}}\right) = \log\left[\frac{I(3727)}{I(\mathrm{H}\beta)}\right] + 5.992 + \frac{1.583}{t} - 0.681\log t + \log(1 + 0.00023n). \quad (3)$$

In the case of 11 out of the 12 very low metallicity H II galaxies identified by Kniazev et al. (2003) and also for a subsample of 183 H II galaxies compiled from Izotov et al. (2006), which have no data on the [O II] λ 3272 Å line, the O^+ abundances have been measured from the emission lines of [O II] at 7319 and 7330 Å using the following expression:

$$12 + \log\left(\frac{\mathrm{O^+}}{\mathrm{H^+}}\right) = \log\left[\frac{I(7325)}{I(\mathrm{H}\beta)}\right] + 6.895 + \frac{2.44}{t} - 0.58\log t - \log(1 + 0.0047n). \quad (4)$$

For O^{2+} abundances we can use the [O III] emission lines at 4959 and 5007 Å, along with the electron temperature of [O III]:

$$12 + \log\left(\frac{\mathrm{O^{2+}}}{\mathrm{H^+}}\right) = \log\left[\frac{I(4959) + I(5007)}{I(\mathrm{H}\beta)}\right] + 6.144 + \frac{1.251}{t} - 0.55\log t. \quad (5)$$

These two ionic abundances allow us to calculate the total abundance of oxygen in relation to hydrogen via the expression

$$\frac{\mathrm{O}}{\mathrm{H}} = \frac{\mathrm{O^+} + \mathrm{O^{2+}}}{\mathrm{H^+}}. \quad (6)$$

Abundances of Ne^{2+} have been calculated from the [Ne III] emission line at 3869 Å and the electron temperature of [O III] for a subsample of 773 objects:

$$12 + \log\left(\frac{\mathrm{Ne^{2+}}}{\mathrm{H^+}}\right) = \log\left[\frac{I(3869)}{I(\mathrm{H}\beta)}\right] + 6.486 + \frac{1.558}{t} - 0.504\log t. \quad (7)$$

Finally, regarding Ar, we can measure Ar^{2+}, from the [Ar III] emission line at 7136 Å and the electron temperature of [S III] for a subsample of 572 objects using the following expression:

$$12 + \log\left(\frac{\mathrm{Ar^{2+}}}{\mathrm{H^+}}\right) = \log\left[\frac{I(7136)}{I(\mathrm{H}\beta)}\right] + 6.157 + \frac{0.808}{t} - 0.508\log t. \quad (8)$$

It is possible to measure as well the lines of [Ar IV] at 4713 and 4740 Å. Nevertheless, the first one usually appears blended with a line of He I at 4711 Å that is difficult to correct, so it is better to use

the second one to calculate the ionic abundance of Ar^{3+} through the electron temperature of [O III]:

$$12 + \log\left(\frac{Ar^{3+}}{H^+}\right) = \log\left[\frac{I(4740)}{I(H\beta)}\right] + 4.705 + \\ + \frac{1.246}{t} - 0.156\log t. \quad (9)$$

This abundance has been calculated for a subsample of 253 objects with a simultaneous measurement of the [Ar III] and [Ar IV] emission lines.

4 PHOTOIONIZATION MODELS

A large grid of photoionization models has been calculated in order to check the validity of the ICFs for Ne and Ar.

We have used the photoionization code CLOUDY v06.02 (Ferland et al. 1998), taking as ionizing source the spectral energy distributions of O and B stars calculated with the code WM-BASIC (v2.11,[3] Pauldrach, Hoffmann & Lennon 2001). We have assumed spherical geometry, a constant density of 100 particles per cm^2 and a standard fraction of dust grains in the ISM. We have assumed as well that the gas has the same metallicity as the ionizing source, covering the values 0.05, 0.2, 0.4, 1 and 2 $Z_\odot$, taking as the solar metallicity the oxygen abundance measured by Allende-Prieto et al. (2001; $12 + \log(O/H) = 8.69$). The rest of ionic abundances have been set to their solar proportions. A certain amount of depletion has been taken into account for the elements C, O, Mg, Si and Fe, considered for the formation of dust grains in the code. Although it is expected that the dust-to-gas ratio scales with metallicity (Shields & Kennicutt 1995), we have checked that different values of this ratio do not lead to variations in our results about the computed ICFs in quantities larger than the reported errors. Regarding other functional parameters, we have considered different values of the ionization parameter ($\log U = -3.5$, -3.0, -2.5 and -2.0) and the stellar effective temperature ($T_* = 35\,000$, 40 000, 45 000 and 50 000 K). This gives a total of 80 photoionization models to cover the conditions of different ionized gas nebulae. Atomic data, including collision strengths in the models are consistent with those used in the calculation of chemical abundances. We have checked as well the influence of varying dielectronic recombination rate coefficients in the code according to the most recent values (Badnell 2006, and references therein), but we have not found any relevant variation in our results concerning the calculation of ICFs.

5 DISCUSSION

5.1 ICFs

ICFs stand for the unseen ionization stages of each element.

$$\frac{X}{H} = \mathrm{ICF}(X^{+i})\frac{X^{+i}}{H^+}, \quad (10)$$

where X is the element whose ICF is required and X^{+i} is the ionic species whose abundance is calculated by means of the detected emission lines.

In the case of Ne, only the [Ne III] line at 3869 Å is detected in the optical spectrum in a large sample of objects. Since its ionization structure is quite similar to that of oxygen, the following approximation can be used:

$$\frac{Ne^{2+}}{Ne} \approx \frac{O^{2+}}{O} \quad (11)$$

that leads to

$$\mathrm{ICF}(Ne^{2+}) = \frac{O}{O^{2+}} \approx \frac{O^+ + O^{2+}}{O^{2+}}. \quad (12)$$

This relation is shown as a thick dashed line in Fig. 1. Nevertheless, Izotov et al. (2004a) point out from a set of photoionization models that this approximation is less accurate in regions with a lower ionization parameter where the charge-transfer reaction between O^{2+} and H^0 becomes more efficient. In this type of objects, it is expected to find larger abundances of Ne^{2+} in relation to O^{2+} and, hence, the O^{2+}/O ratio provides larger ICFs. This trend is confirmed with the set of photoionization models used by Izotov et al. (2006) that, besides, find a slight dependence of the ICF(Ne^{2+}) on metallicity, with larger values of this ICF for high-metallicity regions. This dependence is due to the addition of X-rays sources in their models with lower metallicity and not to a real dependence on metallicity or ionization parameter. The ICFs from Izotov et al. (2006) are shown as the thin solid lines in Fig. 1. The fit of our models for the hottest stars (45 000 and 50 000 K), whose effective temperatures reproduce better the radiation field in the most-massive ionizing cluster, is shown as a thick solid line in Fig. 1. It reveals the same overestimate of the classical approximation in low-excitation objects. However, we do not find any notable dependence on the metallicity. This fit gives:

$$\mathrm{ICF}(Ne^{2+}) = 0.753 + 0.142x + \frac{0.171}{x}, \quad (13)$$

where $x = O^{2+}/(O^+ + O^{2+})$, with an rms of 0.074 only.

Regarding Ar, the ICF can vary depending on the availibity of Ar^{3+} abundances. Izotov et al. (1994) propose the following formula to calculate the total abundance of Ar using the ionic abundances of

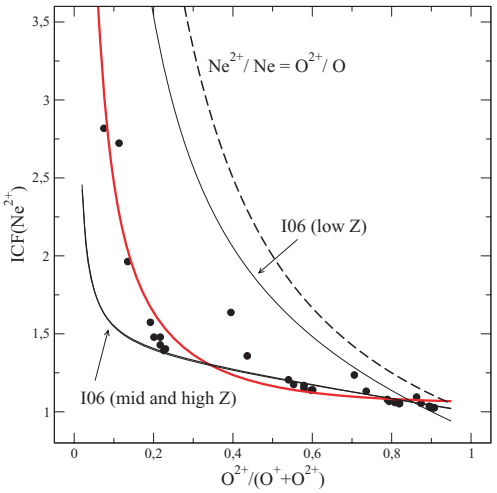

Figure 1. Different relations between the ICF(Ne^{2+}) and the ratio of O^{2+}/O, approximated by $O^{2+}/(O^+ + O^{2+})$. The points correspond to the models described in the text for stellar atmospheres of 45 and 50 kK. The thick solid line represents the best fit to these points. The thin solid lines correspond to different fits of photoionization models as a function of metallicity in Izotov et al. (2006). Finally, the thick dashed line represents the classical approximation.

[3] Available at http://www.usm.uni-muenchen.de/people/adi/Programs/Programs.html.

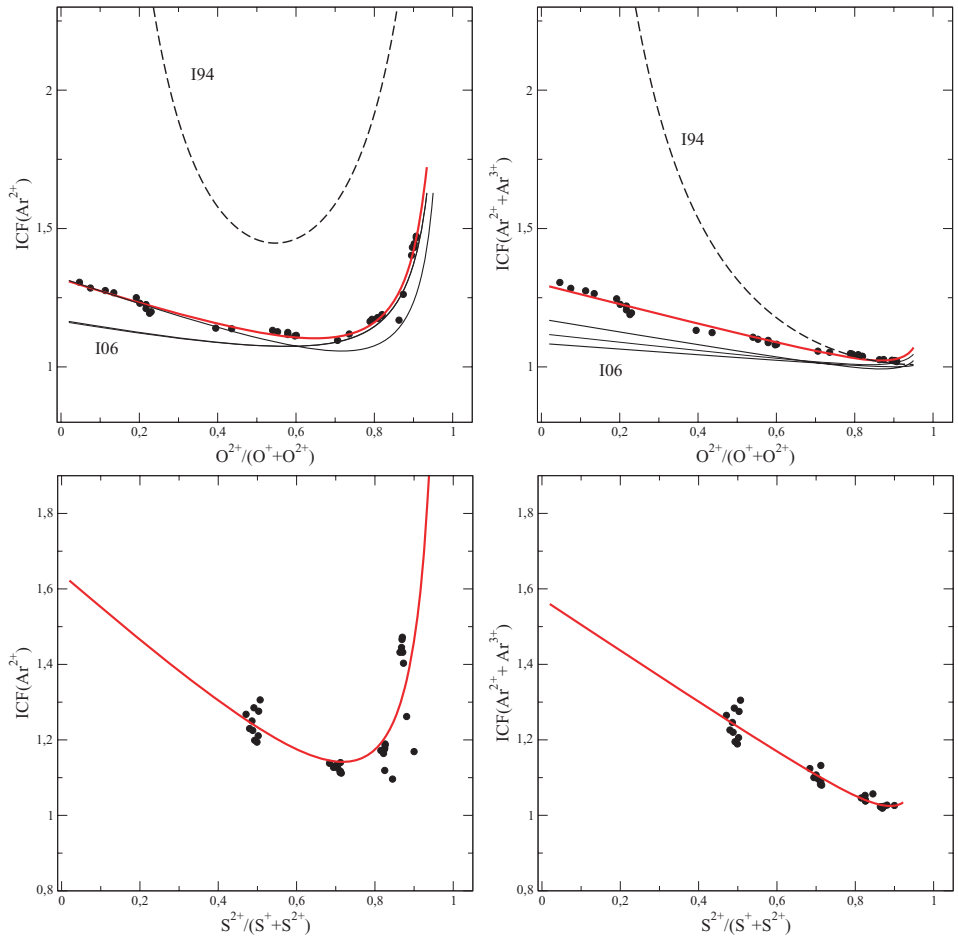

Figure 2. Representation of the ICF for Ar as a function of the $O^{2+}/(O^{+}+O^{2+})$ ratio in the two upper panels, and as a function of $S^{2+}/(S^{+}+S^{2+})$ in the lower ones. The dashed lines represent the expressions given by Izotov et al. (1994), and the thin solid lines represent those in Izotov et al. (2006). Finally, the points represent the models described here for cluster effective temperatures of 45 and 50 kK. The thick line is the best fit to these points.

these two ions:

$$\mathrm{ICF}(\mathrm{Ar}^{2+}+\mathrm{Ar}^{3+}) = \left[0.99+0.091\left(\frac{\mathrm{O}^{+}}{\mathrm{O}}\right) - 1.14\left(\frac{\mathrm{O}^{+}}{\mathrm{O}}\right)^{2}+0.077\left(\frac{\mathrm{O}^{+}}{\mathrm{O}}\right)^{3}\right]^{-1}. \quad (14)$$

On the other hand, if only the emission line of [Ar III] is available, they propose the following expression:

$$\mathrm{ICF}(\mathrm{Ar}^{2+}) = \left[0.15+2.39\left(\frac{\mathrm{O}^{+}}{\mathrm{O}}\right)-2.64\left(\frac{\mathrm{O}^{+}}{\mathrm{O}}\right)^{2}\right]^{-1}. \quad (15)$$

Both formulae are shown as the dashed lines in the two upper panels of Fig. 2, respectively. Nevertheless, these fits clearly overestimate the amount of total Ar compared with the expressions proposed by Izotov et al. (2006) who, as in the case of Ne, find a dependence on metallicity. These fits are shown in the upper panels of Fig. 2 as the thin solid lines for low, intermediate and high metallicities. Finally, the fits to our own models are closer to the latter, but we do not find any relevant dependence of our models on metallicity. The expressions for the fits of these models are, as a function of $x = \mathrm{O}^{2+}/(\mathrm{O}^{+}+\mathrm{O}^{2+})$,

$$\mathrm{ICF}(\mathrm{Ar}^{2+}+\mathrm{Ar}^{3+}) = 0.928+0.364(1-x)+\frac{0.006}{1-x}. \quad (16)$$

with an rms of 0.011, shown as a thick solid line in the left-hand upper panel of Fig. 2, and

$$\mathrm{ICF}(\mathrm{Ar}^{2+}) = 0.596+0.967(1-x)+\frac{0.077}{1-x} \quad (17)$$

with an rms of 0.067, shown as a thick solid line in the right upper panel of Fig. 2. It is possible, as well, to express these ICFs as a function of sulphur abundances. This allows to derive total Ar abundances using red or near-IR observations only, in the case of ICF of Ar^{2+}. Besides, these ICFs can be used in the subsample of SDSS objects whose [O II] line at 3727 Å is not detected but which, on the contrary, have good detection of the [S III] at 9069 Å. The fits of our models, as a function of $x = \mathrm{S}^{2+}/(\mathrm{S}^{+}+\mathrm{S}^{2+})$ are

$$\mathrm{ICF}(\mathrm{Ar}^{2+}+\mathrm{Ar}^{3+}) = 0.870+0.695(1-x)+\frac{0.0086}{1-x} \quad (18)$$

with an rms of 0.019, which is shown as a thick solid line in the left-hand lower panel of Fig. 2, and

$$\mathrm{ICF}(\mathrm{Ar}^{2+}) = 0.596+0.967(1-x)+\frac{0.077}{1-x}, \quad (19)$$

with an rms of 0.068, shown as a thick solid line in the right-hand lower panel of Fig. 2.

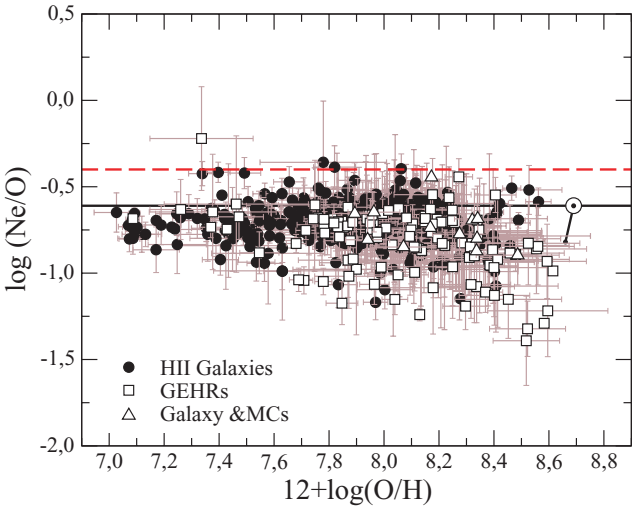

Figure 3. Relation between the abundance ratio Ne/O and the metallicity for the sample of objects described in the text. The solid circles represent H II galaxies, the open squares represent GEHRs and the open triangles represent H II regions in the Galaxy and the Magellanic Clouds. We show as well the solar chemical abundances for O (Allende Prieto et al. 2001) and for Ne (Grevesse & Sauval 1998), linked by a solid line with the solar Ne/O ratio from Asplund et al. (2005). The dashed line represents the ratio calculated by Drake & Testa (2005) for a set of stellar coronae.

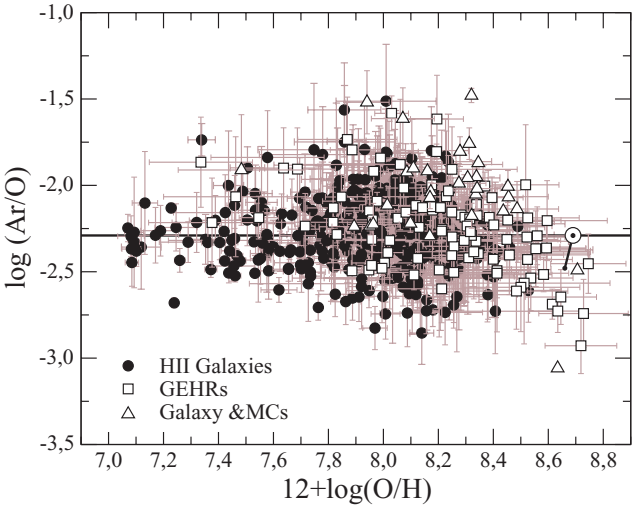

Figure 4. Relation between the abundance ratio Ar/O and the metallicity for the sample of objects described in the text. We show as well the solar chemical abundances for O (Allende Prieto et al. 2001) and for Ar (Grevesse & Sauval 1998) linked by a solid line with the solar Ar/O ratio from Asplund et al. (2005).

5.2 Behaviour of Ne/O and Ar/O with metallicity

We have applied the ICF(Ne^{2+}) derived from our set of photoionization models to a total sample of 578 H II galaxies, 117 GEHRs and 12 H II regions in our Galaxy and the Magellanic Clouds. In Fig. 3, we represent the ratio of Ne/O as a function of the total oxygen abundance, and we compare the obtained values with the solar one, taking the solar oxygen abundance to be 12+log(O/H) = 8.69 (Allende Prieto, Lambert & Asplund 2001) and the solar Ne abundance to be 12+log(Ne/H) = 8.08 (Grevesse & Sauval 1998). Although there is a high dispersion, probably due to chemical inhomogeneities and different observational conditions, the values agree quite well with the assumption of a constant value of Ne/O, at least for low and intermediate metallicities. At higher metallicities, there is a slight decrease in Ne/O with O/H, perhaps due to the underestimate of the corresponding ICF in this regime, as pointed out by Izotov et al. (2006). Nevertheless, since we have not used additional X-ray sources in our models, this problem has to be further investigated. At this point, it is necessary to stress that all the results from photoionization models are in contradiction with Vermeij & van der Hulst (2002) who find Ne^{+} abundances even larger that those predicted by the classical approximation in a set of H II regions in the Galaxy and the Magellanic Clouds from direct *ISO* observations of the emission lines of [Ne II] and [Ne III] in the mid-IR. Regarding the constant value of Ne/O, the average value of the sample, which is -0.72 ± 0.13, is lower, although within the error, than our assumed solar one, but higher than the value reported by Asplund, Grevesse & Sauval (2005), connected to the value assumed here with a solid line in Fig. 3 ($\log(\mathrm{Ne/O}) = -0.82$ in the photosphere). Nevertheless, all the derived values are far from the value found by Drake & Testa (2005) using *Chandra* X-ray spectra in the coronae of 21 stars, which is $\log(\mathrm{Ne/O}) \approx -0.4$. If this value is correct, then there is a clear underestimate of Ne abundances as derived from optical collisional lines.

Regarding the relation between the Ar/O ratio and oxygen abundance, our results are shown in Fig. 4. In order to calculate total Ar chemical abundances, we have used ICFs based on the O^{2+}/O ratio for ($Ar^{2+} + Ar^{3+}$) (104 objects) and Ar^{2+} (344 objects), and ICFs based on the $S^{2+}/(S^{+}+S^{2+})$ ratio for the SDSS galaxies from Izotov et al. (2006) which do not have observation of the [O II] 3727 Å line but for which measurements of the [S III] 9069 Å line exist: 44 galaxies in the case of ($Ar^{2+} + Ar^{3+}$) and 101 in the case of Ar^{2+}. The value of Ar/O presents a larger dispersion than that in the case of Ne/O, with an average value similar to the solar value from Allende Prieto et al. (2001) and Grevesse & Sauval (1998), represented by the solar symbol in Fig. 4 and slightly higher than the value from Asplund et al. (2005), connected to it with a solid line. The relation appears to be slightly different for H II galaxies, whose behaviour is quite similar to that in the Ne/O diagram, and for GEHRs, for which there exists a slight trend of decreasing Ar/O for increasing metallicities. A more careful analysis for individual disc galaxies, as can be seen in Fig. 5, shows this trend more clearly; contrary

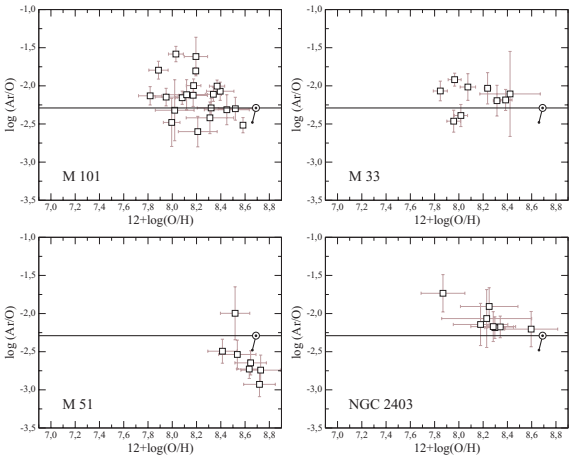

Figure 5. Relation between the abundance ratio Ar/O and the metallicity for the discs of some spiral galaxies. From the left- to right-hand panel and from the top to bottom panel: M101, M51, M33 and NGC 2403.

to it is expected for the production of an α element like Ar. This is compatible with the existence of larger Ar/O at lower effective radius, since there is evidence of negative gradients of metallicity in all these galaxies (M101: Kennicutt & Garnett 1996; M51: Díaz et al. 1991; M33 and NGC 2403: Garnett et al. 1997). This result agrees quite well with that obtained for sulphur, both for extragalactic H II regions (Díaz et al. 1991; Pérez-Montero et al. 2006) and halo metal-poor stars (Israelian & Rebolo 2001).

5.3 Empirical parameters based on Ne and Ar lines

Although the [Ne III] emission line at 3869 Å and the [Ar III] emission line at 7136 Å are fainter than the oxygen emission lines, which are commonly used in different empirical calibrations of chemical abundances, they can be useful to ascertain metallicities when these lines are not available, either because they shift out of the optical region due to the object redshift or because the instrumental configuration does not cover the blue-green region of the spectrum.

The empirical calibrators are commonly used in objects whose low S/N and/or high metallicities do not allow the accurate measurement of any of the auroral lines and, therefore, it is not possible to derive the electron temperature and the ionic chemical abundances from the strong collisional lines.

This is the case for the emission-line ratio I([Ne III] 3869 Å)/I([O II] 3727 Å), proposed by Nagao et al. (2006) as an empirical calibrator useful for high-redshift galaxies (up to $z = 1.6$ in the optical part of the spectrum) and relatively independent of reddening due to the proximity of the two lines. We show in Fig. 6 the relation between this ratio and the oxygen abundance for the sample of objects described in Section 2. This figure shows a very high dispersion in all the metallicity range but which is especially large in the high-metallicity regime. This is confirmed by the objects in the Galaxy and the Magellanic Clouds compiled by Peimbert et al. (2007) for which there exists a direct determination of the oxygen abundance by means of recombination lines. The residuals between the direct

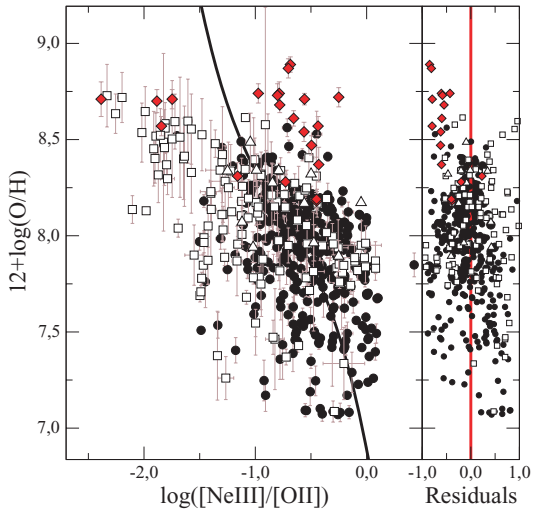

Figure 6. Relation between the logarithm of the ratio of the [Ne III] 3869 Å and [O II] 3727 Å lines and the oxygen abundance for the sample described in Section 2, along with a subsample of objects in our Galaxy and the Magellanic Clouds with oxygen abundance determinations from oxygen recombination lines (solid diamonds). In solid line, it is shown the relation proposed by Nagao et al. (2006) and in the right-hand panel the residuals between the directly derived abundances and those obtained from this calibration.

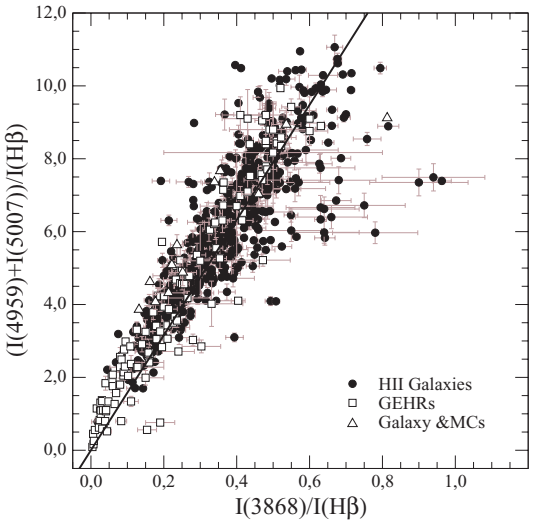

Figure 7. Relation between the intensity of the emission line of [Ne III] at 3869 Å and the sum of the lines of [O III] at 4959 and 5007 Å for the sample of objects described in Section 2. The solid line represents the best linear fit to the sample.

determination of the oxygen abundance and those obtained from the relation based on the [Ne III]/[O II] ratio are shown in the right-hand panel of the same figure. The standard deviation of these residuals in the whole metallicity regime reaches 0.83 dex.

The reason for this huge dispersion can be found in the high dependence of the [Ne III]/[O II] ratio on ionization parameter, as it is stressed by the same authors that propose it. This dependence is due to the tight relation between the flux of [Ne III] and [O III] emission lines (see Fig. 7), as a consequence of the quite similar ionization structure of O^{2+} and Ne^{2+} and the constant value of the Ne/O ratio. The best linear fit between the fluxes of the lines for this sample yields

$$I([\mathrm{O\,III}]4959 + 5007\,\text{Å}) = (15.37 \pm 0.25) I([\mathrm{Ne\,III}]3869\,\text{Å}). \quad (20)$$

Although there is a deviation from this trend for some H II galaxies showing abnormally high values of the line of [Ne III] (e.g. UM382; Terlevich et al. 1991, HS1440+4302, HS1347+3811; Popescu & Hopp 2000), most of the objects are quite close to this relation. Even for the objects with low intensities, which correspond to high-metallicity/low-excitation regions and for which the charge-transfer reaction between O^{2+} and H^0 becomes more important, there exists a very good agreement with this linear fit. A possible cause to the deviation from this relation in some H II galaxies comes from the fact that Ne^+ has an ionization potential 5.85 eV larger than that of O^+ and therefore is more sensitive to the stellar effective temperature, which is higher in these H II galaxies. One of the consequences of this relation is that the [Ne III]/[O II] ratio is, in fact, almost equivalent to [O III]/[O II] which is highly dependent on ionization parameter and effective temperature (Pérez-Montero & Díaz 2005) and presents a lower dependence on metallicity.

The relation between [O III] and [Ne III] can be used as well in all the other diagnostic ratios involving [O III] lines in a similar way. This is the case of the O_{23} parameter, also known as R_{23}, defined by Pagel et al. (1979) as the relative sum of the strong lines of [O II] at 3727 Å and [O III] at 4959 and 5007 Å in relation to Hβ. The relation between this parameter and the oxygen abundance is widely used for objects at large redshifts due to the relatively blue wavelength and high intensities of the involved lines. There exist many

different calibrations of this parameter, whose main drawbacks are well known. (i) Its relation with metallicity is double valued with increasing values of O_{23} for increasing values of metallicity in the low-metallicity regime and with decreasing values of O_{23} for increasing values of metallicity in the high-metallicity regime, requiring external methods to distinguish the upper from the lower branch and with a high dispersion in the middle range, that makes metallicities quite uncertain in the range $8.0 < 12 + \log(O/H) < 8.4$; (ii) the dependence of O_{23} on other functional parameters like ionization parameter or effective temperature. This is solved with the calibration of the parameter as a function of other quantities that reduce this dependence, as in the case of the [O II]/[O III] ratio (Kobulnicky, Kennicutt & Pizagno 1999 from the models of McGaugh 1991) or the P parameter (Pilyugin 2000); and (iii) the lack of objects with directly derived abundances in the high-metallicity regime makes the upper branch calibration to rely heavily on photoionization model results, which differ appreciably depending on the model atmospheres used (Morisset et al. 2004) and the chosen input conditions. Besides, these models predict higher metallicities than those derived from electron temperatures of [N II] or [S III] in inner disc regions (e.g. Bresolin 2007), but not with those derived from oxygen recombination lines. The difficulties found to derive accurate metallicities using this calibration and, in general, all the other empirical relations, make them appropriate to study distributions of metallicity in a statistical way in large surveys of emission-line objects, but they do not offer reliable results for individual determinations.

We can then define a proxy for the O_{23} parameter, using the relation between [O III] and [Ne III] lines, previously discussed:

$$O_{2Ne3} = \frac{I([O\,II]3727\,\text{Å}) + 15.37 I([Ne\,III]3869\,\text{Å})}{I(H\beta)} \approx O_{23} \qquad (21)$$

that is shown in Fig. 8 for the sample described in Section 2. We also show as a solid line the equivalent to the calibration of the O_{23} parameter based on the models of McGaugh (1991), for an average value of the ionization parameter [$\log([O\,III]/[O\,II]) = 1$]. This calibration gives the lowest dispersion in relation with the sample of objects in both the lower and the upper branch (Pérez-Montero & Díaz 2005). We also show the sample of objects with a direct determination of the oxygen abundances based on recombination lines in order to illustrate how this parameter has the same problems as described above for O_{23}. We can redefine the O_{2Ne3} parameter relative to the closest and brightest hydrogen recombination line, Hδ. These lines are closer in wavelength, which makes its relation to be little reddening and flux calibration-dependent, and useful to larger redshifts (up to $z \approx 1.3$):

$$O_{2Ne3'} = \frac{I([O\,II]3727\,\text{Å}) + 15.37 I([Ne\,III]3869\,\text{Å})}{I(H\delta)} \approx O_{23} \frac{I(H\beta)}{I(H\delta)}. \qquad (22)$$

This parameter being equivalent to O_{23}, it suffers from its same problems, with the additional difficulty of being based on weaker lines and therefore, more difficult to measure with good S/N. In the case of the hydrogen recombination line Hδ, it is affected more importantly by the presence of the absorption line due to underlying stellar populations and its measurement has to be carried out carefully (e.g. Hägele et al. 2006).

We show this parameter in Fig. 9 for the sample of objects described in Section 2 and the sample of H II regions with a determination of the oxygen abundance based on recombination lines. We show as well as a solid line the empirical calibration from McGaugh but in this case we take into account the factor Hβ/Hδ in the x-axis. As in the case of O_{23}, it is necessary to distinguish between the upper and lower branch to derive the oxygen abundance from it. In the case of O_{23}, this is usually done by means of the [N II] lines, but they are not available in the blue part of the spectrum. Other possibility is using the [Ne III]/[O II] ratio, although it is very uncertain. From Fig. 7 we can see that while objects with $\log([Ne\,III]/[O\,II]) < -1.0$ probably have high metallicities, the contrary is not true. The residuals of the oxygen abundances derived with these new parameters as a function of the abundances measured using the direct method for both the lower and the upper branches are shown in Fig. 10. Since we can see, as in the case of O_{23}, both the upper and

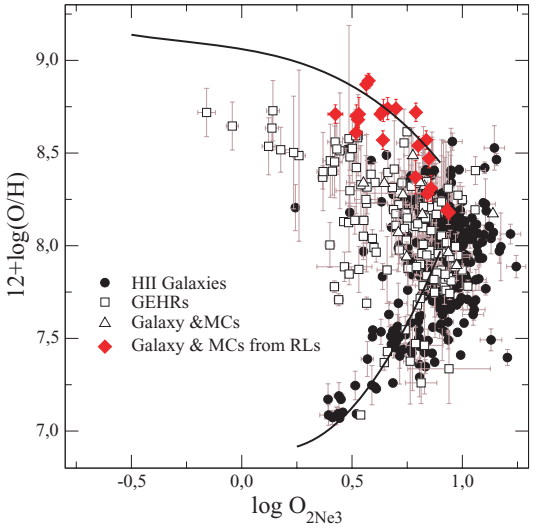

Figure 8. Relation between oxygen abundance and the O_{2Ne3} parameter for the sample of objects described in the text (symbols) and the calibration of McGaugh of the O_{23} parameter for an average value of the ionization parameter ($\log([O\,III]/[O\,II]) = 1$, solid line).

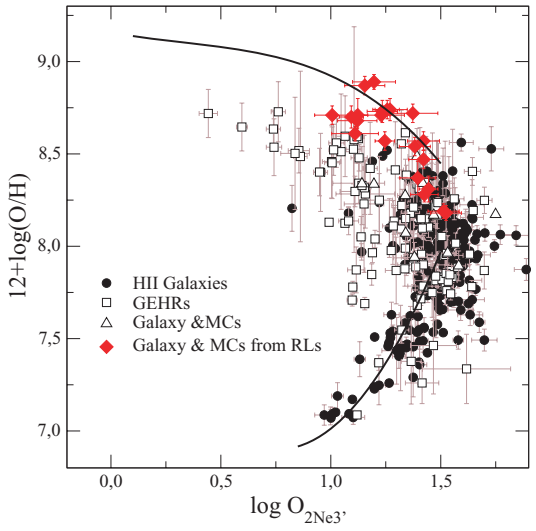

Figure 9. Relation between oxygen abundance and the $O_{2Ne3'}$ parameter for the sample of objects described in the text (symbols) and the empirical calibration of O_{23} of McGaugh for an average value of the ionization parameters ($\log([O\,III]/[O\,II]) = 1$, solid line). This calibration has been displaced in the x-axis by 0.6 dex to take into account the mean value of the Hβ/Hδ ratio.

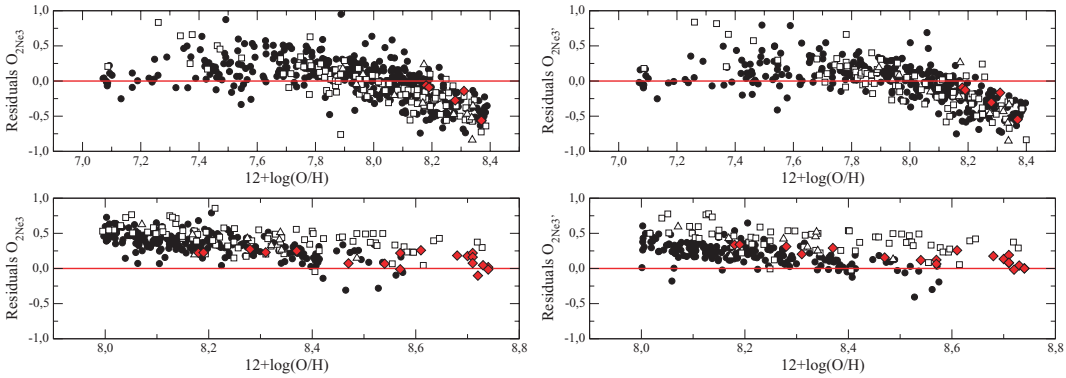

Figure 10. Residuals between the oxygen abundances derived from the McGaugh (1991) calibration of O_{23} applied to O_{2Ne3} (left-hand panel) and to $O_{2Ne3'}$ (right-hand panel) and the oxygen abundances derived from the direct method. The upper panels show the calibration for low metallicities and the lower panels show the calibration for high metallicities.

lower branch calibrations show large differences with the derived metallicities in the turnover region [$8.0 < 12 + \log(O/H) < 8.4$]. The standard deviations of the residuals in the other ranges are quite similar to those obtained for the O_{23} parameter in Pérez-Montero & Díaz (2005) for the McGaugh calibration of the upper branch [0.20 dex for O_{2Ne3} and 0.18 dex for $O_{2Ne3'}$ in the $12 + \log(O/H) > 8.4$ range]. The standard deviations of the residuals between the metallicities derived from the O_{23} parameter are 0.06 dex for both O_{2Ne3} and $O_{2Ne3'}$ parameters. However, in the low-metallicity regime, $12 + \log(O/H) < 8.0$, the dispersion of the residuals in relation with the direct method is 0.24 dex for the O_{2Ne3} parameter and 0.22 dex for the $O_{2Ne3'}$ parameter, which are much higher than the 0.13 dex calculated for the O_{23} parameter in Pérez-Montero & Díaz (2005). In this case the residuals between this calibration and those based on the Ne emission line are 0.14 and 0.16 dex, respectively.

Among the other empirical calibrators based on Ne or Ar emission lines, we can analyse also the Ar_3O_3 parameter, defined by Stasińska (2006) as the ratio of the fluxes of the emission lines of [Ar III] at 7136 Å and [O III] at 5007 Å. In Fig. 11, we show the relation between the oxygen abundances and the logarithm of this parameter for the sample of objects described in Section 2 having a measurement of the [Ar III] line. The standard deviation of the residuals, which are shown in the right-hand panel of the same figure as a function of metallicity, give a value of 0.35 dex. Besides, the behaviour of this parameter in the high-metallicity regime is quite unclear due to the position of some of the objects with a direct determination of the oxygen abundance based on recombination lines, that show lower values of Ar_3O_3 than those expected for their metallicity.

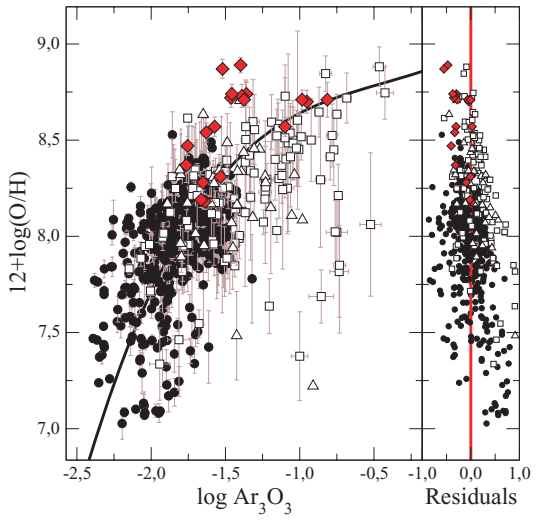

Figure 11. Relation between the Ar_3O_3 parameter and the oxygen abundances derived from the direct method, along with the calibration proposed by Stasińska (2006) for this parameter. In the right-hand panel, we represent the residuals between the directly derived abundances and those derived from the calibration.

5.4 Diagnostic methods for the ionizing source in emission-line objects

Strong lines are used also in emission-line-like objects to find out the nature of the main ionization mechanism: photoionization due to the absorption by the surrounding gas of ultraviolet photons emitted by massive stars, power-law spectral energy distribution associated with AGN or shock excitation. Since some of these diagnostic diagrams for the blue part of the spectrum use the emission lines of [O III] at 5007 and 4959 Å, we could use as well the [Ne III] 3869 Å emission line and the closest and brightest hydrogen recombination line to redefine these diagrams that would be useful up to larger redshifts and would also be less reddening-dependent. This is the case of the relations proposed by Lamareille et al. (2004), as for instance the relation between ([O III] 5007 Å/Hβ) and ([O II] 3727 Å/Hβ). Using the appropriate relations, the analytical expression proposed by these authors take the following expression:

$$\log\left(\frac{[\mathrm{Ne\,III}]3869\,\text{Å}}{\mathrm{H}\delta}\right) = \frac{0.14}{\log([\mathrm{O\,II}]3727\,\text{Å}/\mathrm{H}\delta) - 2.05} + 0.37. \quad (23)$$

In the left-hand panel of Fig. 12, we show this diagram for the objects described in Section 2. Starburst galaxies and star-forming regions lie below the solid line. This diagnostic ratio is, in fact, equivalent to the relation proposed by Rola et al. (1997) between ([Ne III] 3869 Å/Hβ) and ([O II] 3727 Å/Hβ). The rate of coincidences between this diagnostic diagram and its predecessor based on [O III] lines reaches 83 per cent. This diagram can be used also to separate Seyfert 2 galaxies from LINERS using the theoretical expression proposed by Lamareille et al. (2004) adapted for [Ne III] and Hδ:

$$\log\left(\frac{[\mathrm{Ne\,III}]}{\mathrm{H}\delta}\right) = 0.04. \quad (24)$$

All the H II galaxies which present abnormally high values of the emission line of [Ne III] shown in Fig. 7 appear in this diagram in the

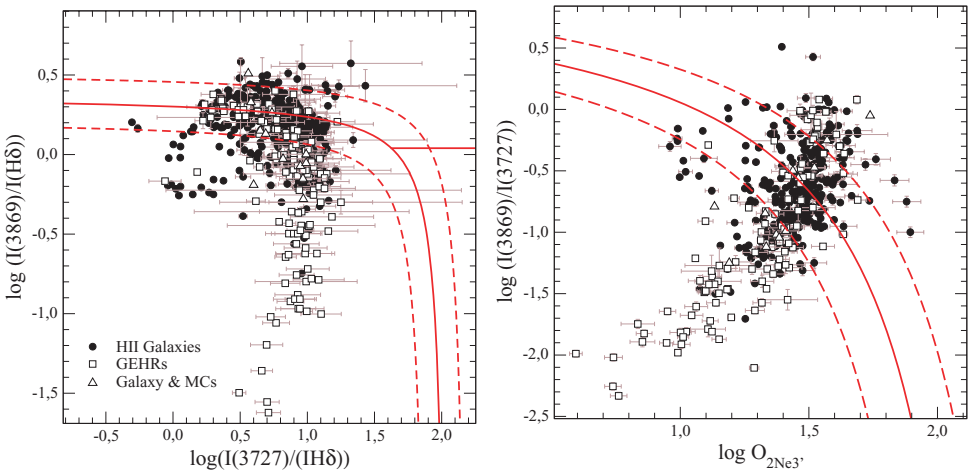

Figure 12. Diagnostic diagrams based on Ne emission lines for the sample of objects described in Section 2. In the left-hand panel, the relation between the ratios [Ne III]/Hδ and [O II]/Hδ is shown and in the right-hand panel the relation between the ratio [Ne III]/[O II] and the $O_{2Ne3'}$ parameter is shown. The solid lines represent the analytical division between star-forming objects and AGN. The dashed lines represent the limit of the bands of uncertainty of 0.15 dex on both sides of each relation.

Seyfert 2 zone, what is consistent with a possibly higher dependence of the [Ne III] line on stellar effective temperature, as it has been previously suggested. This is supported by the fact that any of these galaxies are classified as Seyfert 2 when other diagnostics diagrams, like [S II]/Hα versus [O III]/Hβ or [N II]/Hα versus [O III]/Hβ, are used.

The other blue diagnostic ratio proposed by Lamareille et al. (2004) is the relation ([O III] 4959+5007 Å)/([O II] 3727 Å) versus O_{23}. The analytical expressions proposed by these authors for this diagram can be expressed in terms of [Ne III] and Hδ adopting the form

$$\log\left(\frac{[\mathrm{Ne\,III}]3869\,\text{Å}}{[\mathrm{O\,II}]3727\,\text{Å}}\right) = \frac{1.5}{\log O_{2Ne3'} - 2.3} + 1.21. \quad (25)$$

The diagram is shown in the right-hand panel of Fig. 12 and, again, starburst galaxies and star-forming regions lie below this relation, which is shown as a solid line. Although the rate of coincidences between this relation and the one based on [O II] and [O III] is very high (92 per cent), a larger number of objects are found lying on the AGN region as compared to other diagnostics which somewhat questions its application.

6 SUMMARY AND CONCLUSIONS

We have performed an analysis of a large sample of emission-line objects with a direct determination of the oxygen abundance, via the calculation of the electron temperature, and an accurate measurement of the emission lines of [Ne III] at 3869 Å and [Ar III] at 7136 Å. We have recalculated oxygen, Ne and Ar abundances taking into account the electron temperature most representative for each ionic species. The total chemical abundances have been calculated with the aid of new ICFs for Ne and Ar based on a new grid of photoionization models computed using CLOUDY v06.02 and WM-BASIC stellar model atmospheres.

The new ICF for Ne yields lower abundances for low-excitation objects in relation with the classical approximation $O^{2+}/O \approx Ne^{2+}/Ne$, which does not take into account the charge-transfer reaction between O^{2+} and H^0. This new ICF agrees quite well with the fits proposed by Izotov et al. (2006) for the high- and intermediate-metallicity regime. Nevertheless, although we do not find any relevant dependence of this ICF on metallicity as we have not considered different X-ray sources in our models, there is some evidence of the underestimate of the ICF in the high-metallicity regime. First, the values found by Vermeij & van der Hulst (2002) for a sample of Galactic H II regions from the Ne emission lines in the mid-IR point to larger abundances of Ne^+ in these objects. Secondly, the study of the Ne/O ratio as a function of metallicity shows lower values of Ne/O in the high-metallicity regime. The average value of this ratio agrees better with the solar abundances than the values recently obtained from X-ray observations in stellar coronae (Drake & Testa 2005).

Regarding Ar, we have obtained new ICFs for both Ar^{2+} and Ar^{2+}+Ar^{3+} quite similar to the values found by Izotov et al. (2006) but, again, we do not find any relevant dependence on metallicity. According to these new ICFs, the values proposed by Izotov et al. (1994) clearly overestimate the total abundances of Ar. We propose as well new ICFs based on the ratio $S^{2+}/(S^+{+}S^{2+})$, in order to calculate total Ar abundances using the red and far-IR wavelength range only. The study of the Ar/O ratio as a function of metallicity gives contradictory results for H II galaxies and giant H II regions in spirals discs. For the first ones we find a constant value of the Ar/O ratio, in agreement with the expected results for the stellar production of this element. However, for GEHRs we find evidence for decreasing Ar/O with increasing metallicity. This result is found as well for the S/O ratio both in GEHRs (Díaz et al. 1991; Pérez-Montero et al. 2006) and halo massive stars of our Galaxy (Israelian & Rebolo 2001). Taking into account that the ionization structure of Ar and S are quite similar and that they are produced in the same stellar cores, it is not surprising that their ratios behave in similar ways.

We have studied some empirical parameters of metallicity based on Ne and Ar emission lines. This is the case of the [Ne III]/[O II] ratio proposed by Nagao et al. (2006). We have shown that this parameter is indeed much more sensitive to ionization parameter and effective temperature than to metallicity due to the tight relation existing between [Ne III] and [O III] emission lines. This is due to the constant value of the Ne/O ratio and the identical ionization structures of Ne^{2+} and O^{2+}. In fact [O III] can be substituted by [Ne III] in empirical metallicity calibrations and diagnostic diagrams. This offers the possibility of extending the range of applicability of these

relations to objects with higher redshift minimizing at the same time the effects of reddening corrections and flux calibration. We have then defined an abundance parameter $O_{2Ne3'}$ equivalent to the commonly used O_{23} but using the sum of the [O II] and [Ne III] lines relative to Hδ. Although this parameter has the same problems as O_{23} (double valued, dependence on U, calibration of the upper branch), it constitutes a new tool to derive oxygen abundances in large deep optical surveys of galaxies up to high redshifts ($\approx$1.3). Using the same principle, we have defined new diagnostic methods based only on [O II] and [Ne III], similar to those proposed by Rola et al. (1997), that could be used in the same surveys to separate star-forming galaxies from AGN. The results obtained from these diagrams are very similar to those obtained from the other ones in the blue part of the spectrum.

ACKNOWLEDGMENTS

We would like to thank the referee, G. J. Ferland, for many valuable suggestions and comments which have helped us to improve this paper. This work has been supported by the CNRS-INSU (France) and its Programme National Galaxies and the project AYA-2004-08260-C03-03 of the Spanish National Plan for Astronomy and Astrophysics. Also, partial support from the Comunidad de Madrid under grant S0505/ESP/000237 (ASTROCAM) is acknowledged. ÁID acknowledges support from the Spanish MEC through a sabbatical grant PR2006-0049 and thanks the hospitality of the Institute of Astronomy of Cambridge. GFH acknowledges support from the Spanish MEC through FPU grants and the hospitality of Observatoire Midi-Pyrénées.

REFERENCES

Allende Prieto C., Lambert D. L., Asplund M., 2001, ApJ, 556, L63
Asplund M., Grevesse N., Sauval A. J., 2005, in Barnes III T. G., Bash F. N., eds, ASP Conf. Ser. Vol. 336, Cosmic Abundances as Records of Stellar Evolution and Nucleosynthesis. Astron. Soc. Pac., San Francisco, p. 25
Badnell N. R., 2006, A&A, 447, 389
Bresolin F., 2007, ApJ, 637, 751
Bresolin F., Garnett D. R., Kennicutt R. C., Jr, 2004, ApJ, 615, 28
Bresolin F., Schaerer D., Gonzàlez Delegado R. M., Stasińska G., 2005, A&A, 441, 981
Butler K., Zeippen C. J., 1994, A&AS, 108, 1
Crockett N. R., Garnett D. R., Jacoby G., 2006, ApJ, 637, 741
De Robertis M. M., Dufour R. J., Hunt R. W., 1987, JRASC, 81, 195
Díaz A. I., Terlevich E., Vilchez J. M., Pagel B. E. J., Edmunds M. G., 1991, MNRAS, 253,
Drake J. J., Testa P., 2005, Nat, 436, 525
Ferland G. J. Korista K. T., Verner D. A. Ferguson J. W. Kingdon J. B., Verner E. M., 1998, PASP, 110, 761
Galavis M. E., Mendoza C., Zeippen C. J., 1995, A&AS, 111, 347
Garnett D. R., 1992, AJ, 103, 1330
Garnett D. R., 2002, preprint (astro-ph/0211148)
Garnett D. R., Shields G. A., Skillman E. D., Sagan S. P., Dufour R. J., 1997, ApJ, 489, 63
Garnett D. R., Kennicutt R. C., Jr, Bresolin F., 2004, ApJL, 607, L21
Grevesse N., Sauval A. J., 1998, Space Sci. Rev., 85, 161
Guseva N. G., Papaderos P., Izotov Y. I., Green R. F., Fricke K. J., Thuan T. X., Noeske K. G., 2003a, A&A, 407, 75
Guseva N. G., Papaderos P., Izotov Y. I., Green R. F., Fricke K. J., Thuan T. X., Noeske K. G., 2003b, A&A, 407, 91
Guseva N. G., Papaderos P., Izotov Y. I., Green R. F., Fricke K. J., Thuan T. X., Noeske K. G., 2003c, A&A, 407, 105
Hägele G. F., Pérez-Montero E., Díaz Á. I., Terlevich E., Terlevich R., 2006, MNRAS, 372, 293
Hägele G. F., Dìaz A. I., Terlevich R., Pèrez-Montero E., Cardaci M. V., 2007, MNRAS, submitted
Henry R. B. C., 1989, MNRAS, 241, 453
Israelian G., Rebolo R., 2001, ApJ, 557, L43
Izotov Y. I., Thuan T. X., 1998, ApJ, 497, 227
Izotov Y. I., Thuan T. X., 2004, ApJ, 602, 200
Izotov Y. I., Thuan T. X., Lipovetsky V. A., 1994, ApJ, 435, 647
Izotov Y. I., Lipovetsky V. A., Chaffee F. H., Foltz C. B., Guseva N. G., Kniazev A. Y., 1997, ApJ, 476, 698
Izotov Y. I., Chaffee F. H., Foltz C. B., Green R. F., Guseva N. G., Thuan T. X., 1999, ApJ, 527, 757
Izotov Y. I., Chaffee F. H., Green R. F., 2001, ApJ, 562, 727
Izotov Y. I., Papaderos P., Guseva N. G., Fricke K. J., Thuan T. X., 2004a, A&A, 421, 539
Izotov Y. I., Stasińska G., Guseva N. G., Thuan T. X., 2004b, A&A, 415, 87
Izotov Y. I., Stasińska G., Meynet G., Guseva N. G., Thuan T. X., 2006, A&A, 448, 955
Kennicutt R. C. Jr, Garnett D. R., 1996, ApJ, 456, 504
Kniazev A. Y., Grebel E. K., Hao L., Strauss M. A., Brinkmann J., Fukugita M., 2003, ApJ, 593, L73
Kobulnicky H. A., Kennicutt R. C. Jr, Pizagno J. L., 1999, ApJ, 514, 544
Lamareille F., Mouhcine M., Contini T., Lewis I., Maddox S., 2004, MNRAS, 350, 396
Lee J. C., Salzer J. J., Melbourne J., 2004, ApJ, 616, 752
Lennon D. J., Burke V. M., 1994, A&AS, 103, 273.
McGaugh S. S., 1991, ApJ, 380, 140
Melbourne J., Phillips A., Salzer J. J., Gronwall C., Sarajedini V. L., 2004, AJ, 127, 686
Morisset C., Schaerer D., Bouret J.-C., Martins F., 2004, A&A, 415, 577
Nagao T., Maiolino R., Marconi A., 2006, A&A, 459, 85
Pagel B. E. J., Edmunds M. G., Blackwell D. E., Chun M. S., Smith G., 1979, MNRAS, 189, 95
Pauldrach A. W. A., Hoffmann T. L., Lennon M., 2001, A&A, 375, 161.
Peimbert M., Peimbert A., Esteban C., Garcia-Rojas J., Bresolin F., Carigi L., Ruiz M. T., Lopez-Sanchez A. R., 2007, in Guzmán R., Pachham C., Rodríguez-Espinosa J. M., Torres-Peimbert S., eds, Rev. Mex. Astron. Astrofis. Ser. Conf. Vol. 29, First light Science with the GTC. UNAM, Mexico, p. 72
Pérez-Montero E., Díaz A. I., 2003, MNRAS, 346, 105
Pérez-Montero E., Díaz A. I., 2005, MNRAS, 361, 1063
Pérez-Montero E., Díaz, Á. I., 2007, MNRAS, 377, 1195
Pérez-Montero E., Díaz A. I., Vílchez J. M., Kehrig C., 2006, A&A, 449, 193
Pilyugin L. S., 2000, A&A, 362, 325
Popescu C. C., Hopp U., 2000, A&AS, 142, 247
Pradhan A. K., 1976, MNRAS, 177, 31.
Ramsbottom C. A., Bell K. L., Stafford R. P., 1996, At. Data Nucl. Tab, 63, 57
Rola C. S., Terlevich E., Terlevich R. J., 1997, MNRAS, 289, 419
Tayal S. S., Gupta G. P., 1999, ApJ, 526, 544
Shaw R. A., Dufour R. J., 1995, PASP, 107, 896
Shields J. C., Kennicutt R. C., 1995, ApJ, 454, 807
Stasińska G., 2006, A&A, 454, L127
Storey P. J., Hummer D. G., 1995, MNRAS, 272, 41
Terlevich R., Melnick J., Masegosa J., Moles M., Copetti M. V. F., 1991, A&AS, 91, 285
van Zee L., 2000, ApJ, 543, L31
Vermeij R., Damour F., van der Hulst J. M., Baluteau J.-. P., 2002, A&A, 390, 649
Vermeij R., van der Hulst J. M., 2002, A&A, 391, 1081
Weaver T. A., Woosley S. E., 1993, Phys. Rev., 227, 65
Zeippen C. J., Le Bourlot J., Butler K., 1987, A&A, 188, 251

This paper has been typeset from a TEX/LATEX file prepared by the author.